WiSh: Towards a Wireless Shape-aware World using Passive RFIDs

Haojian Jin*, Jingxian Wang*, Zhijian Yang, Swarun Kumar, Jason Hong
Carnegie Mellon University
Pittsburgh, PA
{haojian@cs.,jingxian@,zhijian1@andrew.,swarun@,jasonh@cs.}cmu.edu

ABSTRACT

This paper presents WiSh, a solution that makes ordinary surfaces shape-aware, relaying their real-time geometry directly to a user's handheld device. WiSh achieves this using inexpensive, light-weight and battery-free RFID tags attached to these surfaces tracked from a compact single-antenna RFID reader. In doing so, WiSh enables several novel applications: shape-aware clothing that can detect a user's posture, interactive shape-aware toys or even shape-aware bridges that report their structural health.

WiSh's core algorithm infers the shape of ordinary surfaces using the wireless channels of signals reflected off RFID tags received at a single-antenna RFID reader. Indeed, locating every RFID tag using a single channel measurement per-tag is challenging, given that neither their 3-D coordinates nor orientation are known a priori. WiSh presents a novel algorithm that models the geometric constraints between the coordinates of the RFID tags based on flexibility of the surface upon which they are mounted. By inferring surface curvature parameters rather than the locations of individual RFID tags, we greatly reduce the number of variables our system needs to compute. Further, WiSh overcomes a variety of system-level challenges stemming from signal multipath, stretching of fabric and modeling large surfaces. We implement WiSh on commodity RFID readers and tags attached to a variety of surfaces and demonstrate mm-accurate shape-tracking across various applications.

CCS CONCEPTS

• **Human-centered computing** → **Ubiquitous and mobile computing systems and tools**;

KEYWORDS

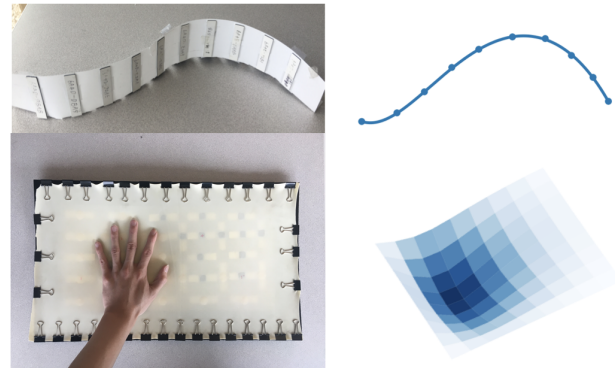RFID sensing, shape-aware, smart fabric, smart material

Figure 1: WiSh takes as input wireless channel measurements from a 2-D surface (or 1-D string) instrumented with passive RFID tags and outputs the shape of the corresponding surface (or curve).

1 INTRODUCTION

Imagine a world where every surface around us is shape-aware, relaying its precise and real-time geometry to our handheld device. Such a system can fundamentally change the way we interact with surfaces in our vicinity. Imagine smart fabrics that infer the curvature of our spine to track our posture when we exercise. Or consider objects that we grasp – plush toys, computer peripherals and exercise equipment, responding differently based on how and where they are depressed. At a larger scale, consider bridges that measure their sag-over-time [34] to track the structure health.

While there has been much past work on shape sensing, using them to make all surfaces around us shape-aware poses a challenge. On one hand, infrastructure-based solutions such as depth cameras[37] function only in environments where they are deployed and must be in line-of-sight to the surface sensed. On the other hand, recent efforts to build shape aware materials using advanced motion sensors [9, 57] are expensive ($100 per meter), bulky and need batteries that have to be frequently recharged.

We present WiSh, the first wireless shape sensing solution that allows users with a compact single-antenna RFID reader to track the shape of surfaces around them instrumented with inexpensive RFID tags. Passive RFID tags are battery-free, machine-washable, lightweight, flexible and cost a few cents, making them an ideal shape-sensing technology for a wide-range of everyday surfaces

Haojian Jin*, Jingxian Wang*, Zhijian Yang, Swarun Kumar, Jason Hong

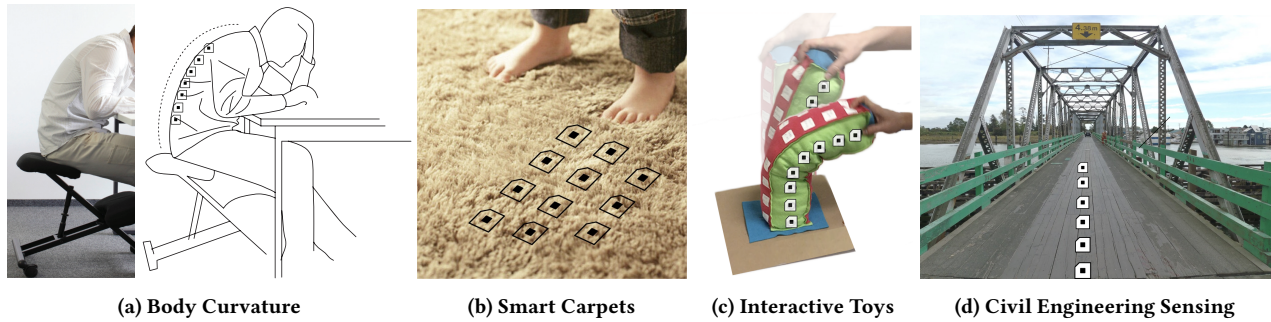| (a) Body Curvature | (b) Smart Carpets | (c) Interactive Toys | (d) Civil Engineering Sensing |

Figure 2: Shape-aware surface examples instrumented with passive RFID tags: (a) smart fabrics that can track the posture of a user in real-time as they carry on with their daily activities; (b) smart carpets that detect the presence and locations of users on them by tracking where they are depressed; (c) interactive toys instrumented with RFID tags can respond differently depending on where they are touched and with what level of force; (d) bridges can measure their sag-over-time to track the structure health.

and fabrics. WiSh can be applied to any surface around us by weaving the tags into the fabric (e.g. clothing, carpets) or attaching the tags to the object surface (e.g. bridges) (Fig. 2). These tags can then be tracked from a mobile single-antenna RFID-reader that can fit into the user's pocket or be attached to a moving vehicle. The RFID reader can be recharged periodically akin to a user's smartphone and may even be integrated directly into future smart-phones [18].

At first glance, one might consider sensing the geometry of surfaces augmented with RFIDs by using wireless localization. Specifically, one can localize the relative position of individual RFID tags to reconstruct surface geometry. Unfortunately, localizing each RFID tag accurately using a portable handheld device is challenging. State-of-the-art solutions to track RFIDs require multi-antenna RFID readers [50] too bulky for users to carry around. More recent solutions that use a single-antenna reader [21, 42, 52] can at best infer the orientation of an array of tags – not their individual locations. Indeed, the underlying problem of localizing RFID tags with a single-antenna reader is fundamental: A single-antenna RFID reader reports only one phase measurement per-tag, which is insufficient to infer its entire 3-D (x, y, z) coordinates. This is the classic problem of too many variables and too few equations.

In contrast, WiSh addresses this challenge by not localizing individual tags in the first place – instead, tracking the shape of the fabric they are attached to. Specifically, WiSh formulates mathematical models of fabrics and surfaces (higher-order Bézier curves [11]) that represent 2-D surfaces of any material by equations with a small number of unknown coefficients. Since fabrics and surfaces of a given material have known limits on curvature and stretch, the number of these unknown coefficients is far fewer than the number of RFID tags. We then find the optimal coefficients that best fit the observed wireless channels from the tags. By directly optimizing for surface coefficients, as opposed to attempting to find each tag's location, we greatly reduce the number of variables our system needs to infer.

The rest of this paper describes our solutions to the key challenges that increase the number of variables WiSh must compute. First, we must account for the multiple paths of the signals from the RFID reader to the tags as they reflect off walls, furniture, and even the user's own body. Second, we must account for phase-changes owing to the difference in orientation of adjacent RFID tags as they

distort to different curvatures. Finally, we develop a curve stitching technique to scale shape sensing to more complex and larger objects, such as bridges and buildings.

Scope and Limitations: Our paper is an exploratory work that studies and operates under two assumptions driven by industry trends: future RFID readers would be mobile and compact, e.g., integrated into future smartphones [18]; RFID tags can be readily integrated with future textiles using conductive yarns [30, 47]. In this paper, we envision a new RFID architecture where the environment would be massively instrumented with passive RFID tags, and the RFID reader would be mobile.

Since the hardware technology is not well developed yet, there are important limits to the current WiSh implementation. First, it cannot infer wrinkles or twists in fabric that are smaller than the size of one RFID tag (three cm). Second, it cannot obtain folds in RFID tags that cause one RFID to be placed atop another and cause near-field coupling. We detail the limits of WiSh in §10.

We implement WiSh prototypes using commercial passive RFID tags and a commodity Impinj RFID-reader that is connected to a single antenna. We mount arrays of tags on surfaces of different materials and dimensions, and track their curvature and stretch in a variety of settings. As a baseline, we use a fiducial tracking system with two cameras. Our results reveal the following:

- A median displacement of the observed from the true geometry of 17 mm for a 40 cm 1-D string and 24 mm for a 30 cm × 40 cm 2-D surface.
- A 87% accuracy in location-of-touch in a 3-D touch-sensitive smart surface.

Contributions: Our main contribution is a novel solution for ubiquitous shape sensing using passive low-cost RFIDs attached to object surfaces. WiSh achieves this using a single RFID reader whose location or movement does not need to be calibrated.

Our specific contributions are as follows:

- An RFID-based shape-sensing primitive that can measure the precise geometry of a string (1D) or surface (2D). Our approach accounts for the multiplicity of RF signal paths from the RFID tags to the reader.
- A solution that allows both the RFID reader and tags to move relative to each other at unknown trajectories without prior calibration.

- A detailed implementation and evaluation of WiSh across different RFID-array configurations and surfaces to demonstrate high accuracy in shape-sensing.

2 RELATED WORK

Related work falls under three broad categories: shape-sensing infrastructure, smart fabrics and RFID sensing.

Shape Sensing Infrastructure: There has been much past work on developing external infrastructure to sense the shape of observed objects. Depth cameras [19] and LIDARs [31] have long been deployed to scan the 3-D surface of objects in direct line-of-sight at mm-accuracy. Structure-from-motion techniques in computer vision [29] and RF imaging [61] reconstruct the 3-D surface of objects using images captured from multiple vantage points. More recent vision-based systems use commodity cameras coupled with objects labeled with 3-D bar codes to accurately learn the shape of an object even from a single image [3]. There have also been 3-D imaging solutions using ultra-wide band RADAR that require instrumenting the environment with multiple large antennas [28].

At a larger scale, sensing the shape of large structures such as bridges requires special instruments such as inclinometers [59] and highly sensitive motion sensors designed for structural health monitoring [6]. In contrast to the above, our system only requires attaching inexpensive, light-weight and battery-free RFID tags to any surface that is sensed. WiSh can then accurately sense the shape of these surfaces using a handheld RFID reader even if it is in non-line-of-sight relative to them (e.g. in the user's pocket).

Smart Fabrics & Materials: The most straightforward approach to measure fabric deformations is deploying the sensors on the textile directly [40, 44, 60]. For example, FlexSense [40] uses piezo-electric sensors to sense the applied mechanical stress and reconstruct 2.5D surface deformations eventually. However, all these systems require batteries and electronics in the textile which add to the cost and are hard to maintain. In contrast, WiSh tracks shape deformations using low-cost, lightweight, waterproof, battery-free RFID tags.

Designing non-intrusive fashion and aesthetic smart fabrics is another emerging topic [12, 38, 58]. Project Jacquard [38] uses conductive yarns to weave the touch and gesture-sensitive areas on the textile in a non-intrusive way. Biologic [58] takes advantage of the hygromorphic phenomenon in living cells to build electronics-free and wireless fabric materials. Several other recent advances have developed touch-sensitive fabrics [36, 41], stretch-detecting bands [8, 13] and fabric-based user interfaces [22, 60]. While these material science breakthroughs are promising, their sensing capability is restricted to specific types of inputs – touch and humidity, respectively, not shape. In contrast, WiSh provides general geometry sensing in a non-intrusive way using RFIDs. Moreover, WiSh is complementary to most smart fabric techniques by embedding an extra RFID layer [35] to add shape-sensing capabilities.

RFID Sensing: Unlike traditional signal strength based schemes [5, 20, 33], recent RFID localization systems [25, 42, 50, 56] track the RFID tags based on the low-level phase information of backscattered radio waves and achieve cm-level accuracy. However, these systems often require a large antenna array of reader antennas [27, 50, 56]

to perform triangulation and locate the tag. Such multi-antenna readers are too bulky to be used as handheld systems.

Recent systems investigate the use of single antenna RFIDs for a variety of sensing goals. One common goal is to enable discrete gesture classification through analyzing the phase information using machine learning [10, 23, 24, 26]. Some recent systems use a single-antenna reader to infer the orientation of rigid objects [52] or track the angles of joints [21]. More recently, Rio [39] uses the technique of impedance tracking to track users' finger touch movements on RFID tags. RFIDs have also been employed for health sensing. For example, TagBreathe [16] uses a zero-crossing technique to count breathing periods, however assumes a static user in front of a static RFID reader antenna. In contrast, WiSh is designed to provide a generic technique for rich continuous shape tracking. Besides, it tackles a problem different from prior solutions [16, 27, 52], as the position of the reader is unknown and the reader is mobile.

3 AN OVERVIEW OF WISH

WiSh aims to measure the geometry of a 1-D string or 2-D surface instrumented with light-weight, inexpensive and passive RFID tags. The wireless channels from these RFIDs are measured relative to a compact reader with only one antenna at unknown trajectories. In each geometry computation, WiSh obtains only one unique channel measurement per-RFID tag.

These design considerations stem from three reasons. First, the RFID reader in the user's pocket can move with time as the user moves about. Second, the positions of RFID tags may change over time as the surface deforms or moves. Third, using only one antenna reduces the cost, deployment effort, and form factor.

Extracting quasi-simultaneous signals: WiSh uses a sliding window technique [21] to extract the quasi-simultaneous readings for different tags from the data stream. All the tag readings need to occur in a time span of 0.1 seconds. If the sliding window does not include all the tag readings and the 0.1-second duration expired, WiSh will execute based on the partial observations. In practice, some of the tags may become invisible due to occlusion from the body or other object. Our algorithms can then run on the partial sensor array data at the expense of some accuracy.

Modeling the Surface: At this point, WiSh needs to infer the geometry of the surface using one wireless channel per tag. As mentioned previously, one channel measurement is insufficient to find the full 3-D coordinates and orientation of each tag using wireless localization. In contrast, WiSh exploits the fact that the locations of RFID tags are not independent – they lie on a surface whose geometry is constrained by the properties of the underlying fabric or material. Specifically, we model any surface by the equation $S(p) = 0$, where p are a set of parameters that fully define the surface geometry. We constrain the parameters p to only allow for surfaces that stretch or curve to the extent that the material, the surface is made of, supports. We then find the set of parameters p that best fit the observed wireless channels per tag. By choosing functions $S(p)$ that succinctly express surfaces using a small number of elements of p, one can ensure that the size of p is significantly smaller than the number of tags on the surface. Consequently, we can optimize for p to fit the observed channels, even with only one channel measurement per-tag.
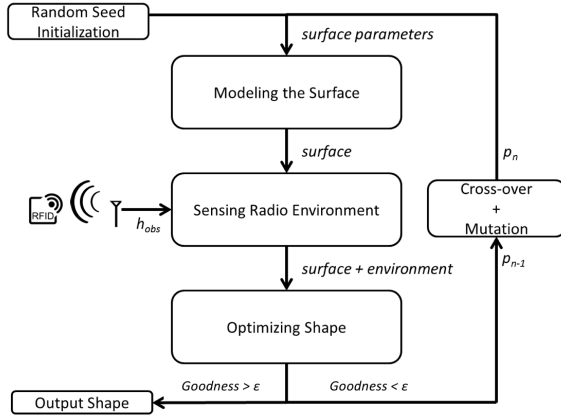
Figure 3: WiSh's shape sensing workflow contains the following steps: (1) We begin with a randomly chosen first-generation of surfaces and model them to find RFID tag locations; (2) We infer the radio environment parameters that best fit the observed channel for each candidate shape; (3) We then estimate the goodness-of-fit of each shape to the observed channels. The best shapes are now passed on to the next generation after a cross-over and mutation phase. The algorithm terminates once a shape with a sufficiently high goodness-of-fit is found.

Radio Environment: Besides the shape of the surface $S(p)$, the observed channels also depend on the radio environment between the RFID reader and tag. We define the radio environment E as a vector composed of three specific properties: (1) Any phase shift introduced by the RF-front end at the RFID reader; (2) The attenuations and phase shifts introduced by the multiple signal paths that the signals experience between the reader and tag, as they reflect off walls, furniture, the user's body, etc.; (3) Any phase shift introduced at the RFID tag, particularly due to the orientation of the RFID tag. These unknown values constitute additional variables our system must optimize over in order to find the shape of the surface.

Shape Optimization: WiSh's optimization problem aims to find the surface parameters p that best fit the observed channels. Mathematically, let h_{obs} denote the observed channels from each RFID tag and $h_{est}(S(p), E)$ denote the estimated channels based on the geometry of the surface $S(p)$, we aim to track and the radio environment E (as described above). We then wish to compute:

$$p^* = \arg\min_{p} \min_{E} \sum ||h_{est}(S(p), E) - h_{obs}||^2 \qquad (1)$$

The above objective function is non-convex, ruling out most gradient-based approaches to solve the optimization. Indeed, we empirically find that the objective function, while continuous, has a large number of local minima. This makes solving the optimization efficiently and accurately, short of enumerating all possible radio environments and shapes, a challenging task.

WiSh addresses the above challenge by using a genetic algorithm [54], an approach to solve non-convex optimizations efficiently inspired by natural selection. Our algorithm begins with a

population of surfaces with randomly-generated parameters called the first generation. We then proceed with the following three steps:

- **Modeling the surface:** First, we infer the positions of the RFID tags based on the shape of the surface for each parameter p in the generation. The key challenge in doing so is to define the function $S(p)$ to succinctly describe everyday surfaces and fabrics, while accommodating constraints on their allowed stretch and curvature.
- **Radio Environment:** Next, we find the optimal environment E that fits the observed channels, based on the known shape $S(p)$ for each member of the generation. That is, we must investigate efficient solutions to the following optimization, based on observed wireless channels at an array of RFID tags of arbitrary shape:

$$E^* = \arg\min_{E} \sum ||h_{est}(S(p), E) - h_{obs}||^2 \qquad (2)$$

- **Shape Optimization:** Finally, we find the goodness-of-fit of each member p of the generation defined as:

$$G(p) = 1/\sum ||h_{est}(S(p), E^*) - h_{obs}||^2$$

We only let a small fraction σ of the generation with highest goodness-of-fit survive (where σ is a fixed threshold). We then design efficient approaches to find the next generation through a series of two operations: cross-over that combines two shapes, and mutations that apply random alterations to some shapes. We now repeat the above steps until we find a shape with an acceptably high goodness-of-fit.

Fig 3 visualizes the work flow of WiSh as described above. The rest of this paper (§4-6) describes the challenges and system design decisions in each phase of WiSh above. We further discuss the limitations of our system (§10) as well as a detailed system implementation (§7) and evaluation (§8).

4 MODELING THE SURFACE

In this section, we find a succinct representation of a surface $S(p) = 0$, specified by parameters p, to characterize most surfaces, such as carpets, clothing and toys as well as large surfaces such as bridges. Key to modeling surfaces efficiently is to weave in constraints that limit the maximum stretch and bend that the surface can undergo, based on its material properties.

4.1 Curve and Surface Representation

To model the surface, we seek a representation that can express a large space of natural shapes but requires minimal parameters. Reducing the number of parameters can improve the computational performance and avoid potential over-fitting. Besides, the ideal shape representation capture various material properties, e.g., elongation, stiffness, etc. Finally, the shape representation should also be intuitive for real-world applications, such as touch detection, sag of bridges, spine curvature, etc.

Based on these considerations, we model surfaces using higher-order Bézier curves [2], which are commonly used in graphics to approximate real-world shapes. These curves are routinely used in fabric and textile modeling and analysis [43]. Bézier curves are represented using a series of control points which effectively "pull" (or push) the curve along various directions (i.e., control its tangents).

original   stretch (1.5 times)

bend   bend + stretch (1.5 times)

(a) Bézier Curves
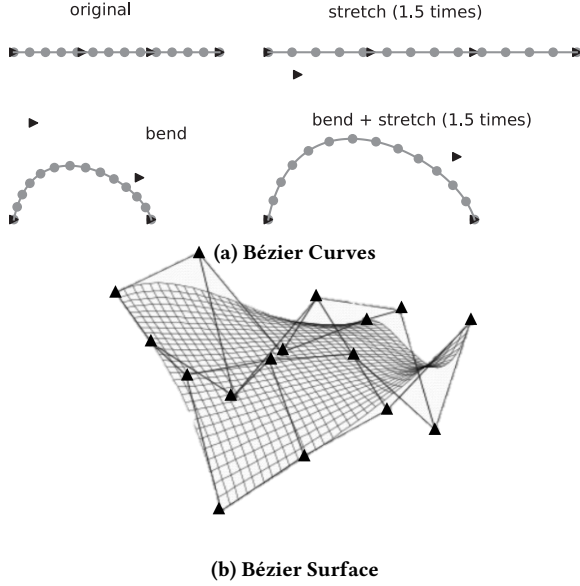
(b) Bézier Surface

Figure 4: Shape examples of curves and surfaces with Bézier control points shown as black triangles. The grey dots (in the curves) and the intersecting points on the grid (on the surface) denote the attached RFID tags.

In effect, this is akin to the effect that users have with common surfaces (fabrics, carpets, bridges, etc.) as they deform different parts of the surface.

A One-Dimensional String: As a starting point, let us consider a one-dimensional string of RFID tags that can deform to various shapes in 2-D space. In general, we can model an nth-order Bézier curve in 2-D space as:

$$S(p = \{\mathbf{C}_i\}, t) = \sum_{i=0}^{n} \binom{n}{i} (1 - t)^{n-i} (t)^i \mathbf{C}_i \qquad (3)$$

where $0 \leq t \leq 1$ and $\mathbf{C}_i$ are the $n + 1$ control points which define the set of parameters p that fully specify the curve. A Bézier curve will always start with the first control point and end with the last control point, while the rest control points dictate the tangents of the curve.

Our implementation uses the cubic (3rd order) Bézier curve (Fig 4) which characterizes most curves on the body (e.g. spine, stomach) as well as most everyday surfaces (e.g. carpets) with the least amount of over-fitting. In such a case, we need four 2D control points to represent the relative shape of an arbitrary string segment $C_0(x_0 = 0, y_0 = 0)$, $C_1(x_1, y_1)$, $C_2(x_2, y_2)$, $C_3(x_3, y_3 = 0)$, resulting in 5 unknown variables. Note that since we only care about the shape of the surface not its location, i.e. the relative coordinates of the control points, as opposed to their absolute location in space, we always set the first control point to the origin and constrain the final control point to lie on the x axis.

We describe our approach to characterize larger and more complex curves or surfaces that require a greater number of parameters below.

A Two-Dimensional Surface: To model 2-D surfaces, our approach uses Bézier surfaces that are a generalization of the Bézier

curve in 3-D space. A general cubic Bézier surface is constructed as the tensor product of two Bézier curves as defined below:

$$S(p = \mathbf{C}_{ij}, u, v) = \sum_{i=0}^{n} \sum_{j=0}^{m} B_i^n(u) B_j^m(v) \mathbf{C}_{ij}, \qquad (4)$$

where each underlying curve is given by:

$$B_i^n(u) = \binom{n}{i} (1 - u)^{n-i} (u)^i, \qquad (5)$$

While the above formulation models complex surfaces due to the large number of control points, in practice, we observe that a smaller number of control points is sufficient over small surface areas. We therefore simplify the above model by using two curves that are univariate blending functions, where the variables u, v are two orthogonal parametric directions. In this formulation, the surface is controlled by two orthogonal curves, each traversing along two orthogonal axes. The control points $\mathbf{C}_{ij}$ in a tensor-product surface are organized topologically into a rectangular array, and the blending functions corresponding to the control points are likewise organized in an array similar to the one in Eqn. 3.

$$S(p = \{\mathbf{C}_i, \mathbf{C}_j\}, u, v) = B_i(u) B_j(v) \mathbf{C}_i \mathbf{C}_j \qquad (6)$$

Larger Curves or Surfaces: To model larger curves formed by structures such as buildings or bridges, a cubic Bézier surface may be insufficient. Simply employing even higher-order curves to address these scenarios may lead to over-fitting, introducing a large number of control points in specific parts of the surface. In contrast, our approach partitions the surface into smaller segments with overlaps, each of which can be modeled as a cubic Bézier surface. We then stitch together the extremities of these segments to recover the shape of the entire surface using the following process that assumes continuity and differentiability of the surface we model: (1) First, we intersect any two surfaces at the RFID tag(s) common to them, typically at their extremities; (2) Second, we rotate the second surface so that the normal vectors to the tangent of the surfaces at the intersecting RFID tag(s) align. By partitioning surfaces into segments in this manner, our approach distributes control points evenly across the entire surface.

4.2 Constraints on Curvature and Stretch

While Bézier curves are an effective formulation to represent a large variety of surfaces, not all of them may obey the constraints of the material that the surface is made of. In particular, we focus on two specific constraints: maximum curvature and stretch. Specifically, rely on well known models of fabric [32, 46] to measure the amount of energy required to deform the shape into any curve, depending on constraints of stiffness and elasticity of the material it is made of. We then eliminate from each generation of Bézier surfaces, any candidates whose required energy exceeds a threshold. In this manner, we weed out outliers whose shapes are unlikely to form in the real-world owing to material constraints.

Modeling Elasticity: Our approach to constrain stretch measures the energy expended to deform the surface into a specific length. Mathematically, we compute the net displacement of each tag away from each other, relative to their prior configuration at the time the

RFIDs were attached to the surface:

$$Q_{elastic} = \sum_{i=0}^{n-1} |d_i - D| \qquad (7)$$

where D is the prior known gap between tags, and d_i is the surface distance between tag i and $i+1$.

Modeling Stiffness: Having computed elasticity, next we compute the energy required in bending the surface into a specific curvature, starting from an initially planar surface. We use a fast energy-based surface wrinkle model [51] to calculate the surface smoothness. Mathematically, we compute the curvature of the Bézier surface by computing the angular rotation between control points. Specifically, let ω_j is the angle formed by the segments connecting control points C_{j-1}, C_j, and C_{j+1}. We then compute:

$$Q_{stiff} = \sum_{i=1}^{n-1} Q(C_i) \qquad (8)$$

$$\text{where } Q(C_i) = \sum_{j=i-1}^{i+1} (e^{-\omega_j} - e^{-\pi}) \qquad (9)$$

When $\omega_j = 0$, Q_{stiff} reaches its maximum when the surface is curved sharply. The energy is fully released when $\omega_j = \pi$, which means a flat surface.

Applying Constraints: At this point, we rely on well-known fabric models to compute the total energy required to distort the surface into a given geometry specified by the Bézier surface parameters [32, 46]:

$$Q_{total} = k_e Q_{elastic} + k_s Q_{stiff} + k_g Q_{gravity} \qquad (10)$$

where k_e, k_s, k_g are elasticity, bending and density constants, respectively. For each surface parameter in any given generation of surfaces in our genetic algorithm, we compute the above energy and eliminate any surfaces whose total required energy exceeds a threshold, thereby rejecting any unrealistic surface geometries (outliers) that our system may output.

Computing Tag Positions: Given any Bézier surface with appropriate constraints on curvature and elasticity (as described above), we now seek to obtain the coordinates of the RFID tags on the surface at its present geometry. For simplicity, we assume that at the time of manufacture the material surface was perfectly planar with the RFID tags placed along a rectangular array with adjacent tags at a known mutual distance D. For any Bézier curve that the surface deforms to, one can then apply a simple geometric projection [48, 49] of the positions of the RFID tags from its initial planar configuration to that of the new geometry. We note that in doing so, we both account for the curvature of the Bézier surface, as well as the stretch that it experiences uniformly over its surface area.

In summary, WiSh's algorithm in the shape-modeling phase performs the following steps: (1) It takes as input a set of surface parameters (i.e. Bézier control points) forming the current generation. At initialization, these parameters are chosen randomly. (2) For each member of the generation, it formulates the Bézier surface (Eqn. 6); (3) It rejects outliers based on allowed curvature and elasticity of the material (Eqn. 10); (4) It then passes on to the next phase, the coordinates of the RFID tags for each surface in the generation, as described above.
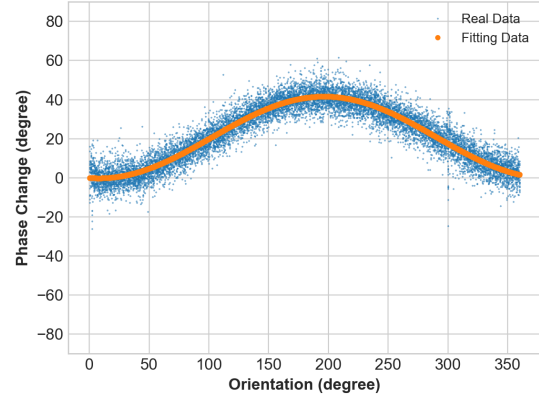

Figure 5: Depicts the phase change (in degrees) of a single RFID tag along different orientations relative to the single-antenna RFID reader.

5 RADIO ENVIRONMENT

Besides the geometry of the surface on which the RFID tags are mounted, the observed wireless channels from RFIDs also depend on the radio environment. In this section, we seek to extract radio environment parameters from the observed wireless channels, for each candidate geometry of the surface. Our algorithm takes as input the current generation of surface geometries as well as the locations of RFID tags upon them, as returned by the surface modeling phase (described in §4 above). We then find the radio environment that best fits the observed channel, for each candidate surface geometry (mathematically formulated in Eqn. 2).

The rest of this section describes our approach to find three components of the radio environment, all of which influence the wireless channels as the signals traverse from the RFID tags to the RFID reader: (1) *Phase shifts at the Tag:* These are primarily produced by change in orientation of the RFID tag that causes shifts in the phase of signals observed from it; (2) *Signal Multipath:* This is the result of the multiple paths the wireless signal from the tag traverses as it reflects off walls, furniture and even the user's body; (3) *Phase shifts at the Reader:* Finally, the radio frontend of the RFID reader introduces an arbitrary phase shift to signals received across RFID tags.

5.1 Effect of Tag Orientation

In an ideal world where RFID tags are perfectly omni-directional point-objects, the orientation of an RFID tags should have no bearing on the phase of the signals it reflects. In practice, however, RFID tags do have specific beam patterns and their orientation in 3-D space can alter the observed phase value at the receiver. In other words, phase offsets due to the orientation of each RFID tag on WiSh's surface of interest are additional variables that our system must infer.

Fortunately, two important properties help us directly estimate this variable per tag by modeling phase shift from tag orientation. First, for any given Bézier surface in a generation, recall that the placement of RFID tags is already known from Sec. 4. Given that
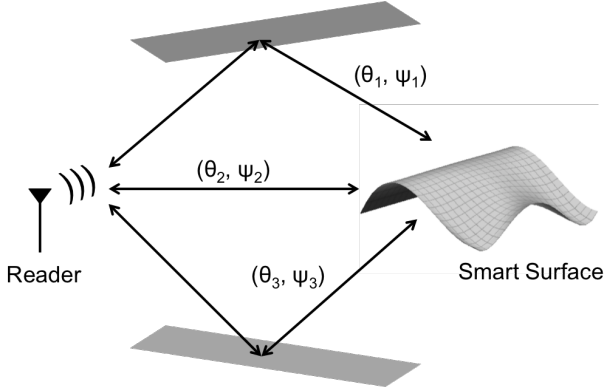
Figure 6: Signals from the RFID tags to the reader traverse along multiple paths as they reflect off various objects in the environment.

the RFID tags we employ are planar with the material surface at the time of manufacture, this means that the orientation of each tag is simply orthogonal to the tangential plane to the surface at the location of the tag. We note that one ambiguity does remain: whether each RFID tag faces "up" or "down" at any time instance. This ambiguity can be eliminated during the time the RFID tags are attached to the surface, by ensuring that all RFIDs are oriented along the same direction a priori. Indeed, during our experiments, we found that this was important to ensure – affixing some RFID tags face-up and others face-down to any surface produces significant errors in our measurements.

Second, one might wonder if the phase shifts introduced by RFID tags can be estimated, even if their orientations are known a priori. Fortunately, RFID tags from the same manufacturer experience predictable phase shifts with change in orientation. Fig. 5 depicts a scatter-plot of the observed phase measurements from thirty OmniID IQ-150 RFID tags measured across orientation. We observe that the relationship between phase shift and orientation is predictable (subject to noise) introducing a small mean error of 10 degrees. We can, therefore, calibrate and compensate for the phase shift introduced by an RFID tag, solely based on its orientation. In other words, phase offsets from the orientation of RFID tags can be corrected for by WiSh, without introducing additional variables to estimate in its optimization.

5.2 Signal Multipath

Next, WiSh must estimate the attenuations and phase shifts experienced by the signal along the different paths the signal traverses as it reflects off various objects in the environment between each tag and reader. Indeed, estimating each of these quantities independently per-tag is infeasible, given that WiSh only has access to one phase measurement per-tag. In contrast, WiSh exploits the fact that adjacent RFID tags will experience similar multipath characteristics owing to their proximity. Specifically, WiSh treats the RFID tags on the surface as an array of antennas. It then applies antenna array algorithms that process the known wireless channels at the array of tags as well as their known geometric configuration (per surface shape in the generation from §4), to separate the various signal paths.

Mathematically, we build on the Multiple Signal Classification (MUSIC) algorithm [55] to perform antenna array processing (Fig. 7). However, recall that unlike traditional antenna arrays which form regular shapes (linear, circular, rectangular, etc.), the RFID tags in WiSh are distorted into arbitrary shapes whose candidate set of geometries are known from §4. As a result, for each candidate tag geometry, we extend the MUSIC algorithm to operate under arbitrary array configurations. We write the power of the received signal from any spatial azimuthal angle θ and polar angle ψ as:

$$P(\theta, \psi) = \frac{1}{|a(\theta, \psi)^{\dagger} E_n E_n^{\dagger} a(\theta, \psi)|} \tag{11}$$

$$\text{where: } a(\theta, \psi) = [e^{4\pi j r_i cos(\theta - \alpha_i) cos(\psi - \beta_i)/\lambda}]_{i=1,\dots,N}$$

Where (r_i, α_i, β_i) are the polar coordinates of the RFID tags, λ is the signal wavelength, j is the square root of -1, E_n are the noise eigenvectors of $h_{obs}h_{obs}^{\dagger}$, h_{obs} represents the vector of observed wireless channels across tags and $(.)^{\dagger}$ is the conjugate-transpose operator. We then estimate the locations of local maxima (peaks) of $P(\theta, \psi)$ to obtain the azimuthal and polar directions-of-arrival: $\{(\theta_k, \psi_k), k = 1, \dots, p\}$ of the p signal paths. At this point, we can obtain the magnitude and phase of the signals corresponding to each path by solving the following optimization:

$$\min_{a_i, \phi_i, \forall k} \sum_{k=1}^{p} ||h_{obs} - a_k e^{-j\frac{\phi_k + 4\pi j r cos(\alpha - \theta_k) cos(\beta - \psi_k)}{\lambda}}||^2 \tag{12}$$

The above is a standard least-squares optimization and can be solved in polynomial-time. We, therefore, apply the least-squares method to obtain for each signal path k, the attenuation a_k and phase shift ϕ_k experienced.

5.3 Phase Shifts at the Reader

Finally, our solution also needs to account for any phase shifts introduced by the RF chains of the RFID reader. Fortunately, since our system uses a single-antenna RFID reader, it introduces only one universal phase shift across all RFID tags. In other words, this is effectively one unknown phase value applied across all RFID tags, across all the signal paths they experience. Mathematically, this phase shift is already captured as an offset to the term ϕ_k obtained from Eqn. 12 and therefore need not be separately computed and accounted for. Said differently, ϕ_k represents both the phase shift introduced by path k as well as the reader.

6 SURFACE OPTIMIZATION

Given a set of candidate surface parameters (a "generation" of surfaces) from §4 as well as their corresponding radio environment parameters from §5, we now aim to formulate a genetic algorithm [54] to optimize for the best candidate surface and iterate over the next generation of candidate surfaces. The genetic algorithm has two phases which we describe below: (1) *Natural Selection:* Among the set of individuals in any generation, only the "fittest" survive. For each shape parameter in the generation, we formulate a goodness-of-fit metric that decides which shapes pass on to the next generation; (2) *The Next Generation:* We then process the individuals that make it past the selection phase to constitute the next generation of shapes. Specifically, we apply two operations: i) Cross-over, which
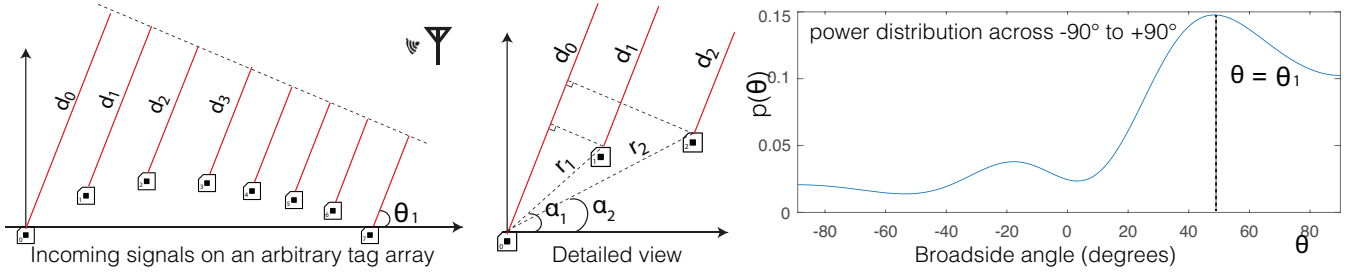
Figure 7: WiSh generalizes the MUSIC algorithm to estimate the angle-of-arrival θ_1 from a single-antenna RFID reader to the tags. This figure illustrates the MUSIC algorithm in 2D space. The tags at a known but arbitrary geometry with polar coordinates (r_i, α_i) as shown. The MUSIC algorithm plots the power of the signal $P(\theta)$ received along each direction θ with a peak(s) at the true direction(s)-of-arrival (θ_1 here).

combines two shapes to result in a hybrid shape; ii) Mutation, which randomly alters the shape.

6.1 Natural Selection

The first step of our optimization is to eliminate shapes that poorly fit the observed channel. To do so, we must formulate a goodness-of-fit metric that takes as input the observed channels, the shape parameters as well as the radio environment (inferred from Sec. 5).

Mathematically, let us consider a shape S whose RFID tags are positioned at polar coordinates are represented as n dimensional vectors: $(\mathbf{r}, \alpha, \beta)$. Let h_{obs} denote the vector of n wireless channels obtained from these tags. In addition, let the azimuthal and polar directions-of-arrival of the signal from the reader be: $\{(\theta_i, \psi_i), i = 1, \ldots, p\}$ for the p signal paths. Let (a_i, ϕ_i) denote the attenuation and phase shift experienced by the signal along each path (from Sec. 5). We write the goodness-of-fit of the candidate shape S as:

$$g(S) = 1 / \sum_{i=1}^{p} ||h_{obs} - a_i e^{-j \frac{\phi_i + 4\pi jr\cos(\alpha - \theta_i)\cos(\beta - \psi_i)}{\lambda}}||^2$$

We then select the top σ fraction ($\sigma = 20\%$ in our implementation) of the shapes based on goodness-of-fit to pass on to the next step.

Convergence: Note that since our optimization culls $(1 - \sigma)$ fraction of the individuals at any given point in time, over time, it is guaranteed to converge in a finite number of steps (in $O(\log_{\frac{1}{1-\sigma}} N)$ steps), where N is the number of individuals initially. Our current implementation converges in around 20 iterations from a randomly chosen seed. Our algorithm is intrinsically also designed to favor individuals that fit the observed channels, resulting in progressive improvements in goodness-of-fit. Our experimental results achieve sub-centimeter error in displacement of surfaces measuring 40cm per-side in 80% of our runs (Fig 9d). We present a detailed experimental evaluation of WiSh in §8.

6.2 The Next Generation

Next, WiSh's genetic algorithm analyzes the goodness-of-fit of individuals in the current generation to check if any are sufficiently low to report. Otherwise, it proceeds to compute the next generation of individuals which are then subsequently processed by phases described above. WiSh performs two biology-inspired operations

on the shapes in each generation: cross-over and mutation, which we describe below.

Crossover: Cross-over is an operation that takes two individuals to compute a hybrid. Cross-over is designed to amplify good characteristics and explore fine-grained solutions. Recall that in WiSh, the parameters of each shape (i.e. each individuals) are a set of control points. Therefore, WiSh performs a cross-over of two shapes by averaging their corresponding control point coordinates. The resulting shape is a hybrid curve that inherits features from both surfaces.

Mutation: Mutation is an operation that introduces random changes in some individuals. Mutation is designed to help the system opportunistically escape from local optima. WiSh performs a mutation by imposing a random offset to one of the control points. We draw this offset from a Gaussian distribution with a standard deviation of D, the mean displacement between the RFID tags.

Algorithm 1 below presents the complete workflow of WiSh's genetic-algorithm based optimization.

Algorithm 1 WiSh Algorithm

1: $\mathbf{P} \leftarrow$ Randomly Initialized set of control points (surface parameter)

Loop:

2: **for** each $p \in \mathbf{P}$ ▷ Control points of one surface
3: $\quad S(p) \leftarrow$ BézierCurve(p) ▷ Sec 4
4: $\quad [\theta, \psi]_{1,\ldots,p} \leftarrow$ MUSIC($S(p), h_{obs}$) ▷ Sec5
5: $\quad [a, \phi]_{1,\ldots,p} \leftarrow$ Least-Square($[\theta, \psi]_{1,\ldots,p}, S(p), h_{obs}$) ▷ Sec5.2
6: $\quad g(p) \leftarrow 1 / \sum_i ||h_{obs} - a_i e^{-j \frac{\phi_i + 4\pi jr\cos(\alpha - \theta_i)\cos(\beta - \psi_i)}{\lambda}}||^2$
7: $Survivors \leftarrow$ top σ members of $\mathbf{P}$ by $g(p)$
8: $\mathbf{P} \leftarrow$ cross-pollinate and mutate ($Survivors$) ▷ Sec6.2

while ($\forall p \in \mathbf{P}; g(p) < threshold$)

return arg max$_{p \in \mathbf{P}} g(p)$

---

7 IMPLEMENTATION

Choice of RFID Tags: Searching for the ideal RFID tags for WiSh was a non-trivial task. First, the human body attenuates radio signals. Although the tags will be attached to the fabric among other surfaces, ideal RFID tags should have a consistent performance

on/off the body. Second, radio sensitivity and directivity are important aspects to consider. If the RFID tag has a strong directivity, the tags can be seldom detected if they do not directly face the reader antenna. Third, ideal RFID tags should have a small and flexible form factor, which can be embedded into clothes and everyday surfaces in a non-intrusive way. After a careful comparison of 20 different types of RFID tags, we use *Omni-ID IQ 150 On-Metal* passive UHF RFIDs in our implementation, which are 1.2 cm × 5.2 cm in size, are light-weight, paper-thin, and have consistent performance on/off the body.

Despite, many battery-powered single-antenna RFID readers available today [18] with up to 12 hours of battery life, these do not provide access to wireless channels (magnitude and phase). Our implementation, therefore, uses the Impinj Speedway RFID reader with a single RFID antenna [7], which reports wireless channels. Our source code is written in Python and C++.

8 EVALUATION

We present a detailed experimental evaluation to understand the performance and limitations of WiSh. Our evaluation varies several key system parameters:

- *Tag spacing*: We test different spacings of the RFID tag array to understand the trade-off between performance and tag density.
- *Signal Multipath*: We examine the impact of multipath on shape sensing accuracy.
- *Fabric materials*: We test different fabric materials in estimating both the stretch and bend to understand WiSh's accuracy and ubiquity.
- *Stress*: We evaluate WiSh under different types of stress (stretch, bend) on 1-D strings and 2-D surfaces.

Apparatus: We build WiSh prototypes on various types of materials: (1) *Paper:* We attach the RFID tags on a 7 cm × 40 cm paper frame to evaluate performance in various multipath-rich settings; (2) *Latex Sheet:* Next, we consider a 0.5 mm thick latex sheet to evaluate system performance under stretch and curvature. We consider two different sheet dimensions: 3 cm × 15 cm and 30 cm × 40 cm. (3) *Fabric (cotton)*: We use a 3 mm thick cotton fabric to evaluate performance with day-to-day clothing. (4) *Woven Conductive Fabrics*: We verify if our system operates even on conductive soft surfaces, generally used to shield electromagnetic signals from the outside.

Performance Metric: To characterize WiSh's performance, we report the absolute error in the position of RFID tags, measured in millimeter on the surface of the fabric. We note that other metrics are also available to measure the shape difference such as a rotation matrix [53]. We choose to use the mean displacement distance since it is a more intuitive measure.

Ground truth: To obtain ground-truth tag positions, we implement a camera-based fiducial tracking system (Fig. 8a) using ARToolKit [3] and affix fiducial markers to our prototypes (Fig. 8b). The ARToolkit calibration program indicates a sub-millimeter baseline accuracy. Based on the fiducial marker tracking results, we perform a surface interpolation [40] to reconstruct the surface's shape and identify ground truth tag positions.
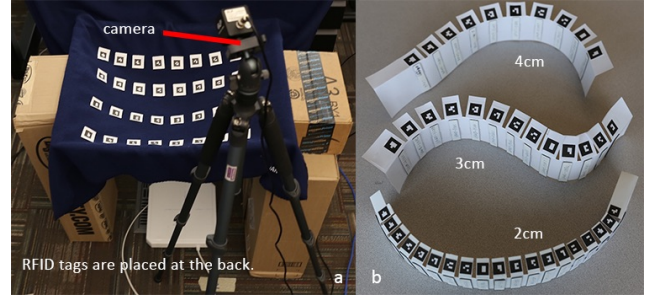

Figure 8: Microbenchmark Apparatus. (a) A camera-based fiducial tracking system; (b) Three shape-aware string prototypes (different tag spacings: 2cm, 3cm, 4cm) using flexible paper platforms for evaluation experiments. We print the fiducial markers on the side to obtain the shape ground truth.

8.1 Tag Spacing

At first blush, one might assume that increasing the number of tags leads to an improvement in accuracy as there are more measurements to rely upon. In practice, however, squeezing the tags too close can be counter-productive owing to inter-tag signal coupling. To understand this trade-off, we conduct experiments by varying the inter-tag spacing.

Method: We built three shape-aware string prototypes by placing Omni ID 150 tags on flexible paper platforms (Fig. 8b). All the prototypes have the same total length (40 cm) but different tag spacings (2cm, 3cm, 4cm), resulting 18, 13, 10 tags respectively. For each prototype, we examine three classes of shapes: concave, convex and wave-like.

To avoid error due to movement of the fiducial markers, we ensure that our setup is static when collecting ground truth data. During the evaluation, the experimenter moves around the prototype in front of the reader antenna (0.5~1 meter away), while the RFID reader and antenna are placed on the floor. We repeat the process three times and collect wireless channel data for each shape. For each shape sensing experiment, we obtain at least 500 independent snapshots (average refresh rate ≈ 16Hz).

Results: Figure 9a illustrates the tag position offsets across the different configurations. The "displacement distance" comes from the errors in both x and y-axis. All three configurations report an average error between 1.3 and 1.9 cm. Among the various configurations, the spacing of 3cm reports a (marginally) higher accuracy. However, the remaining configurations only experience a minor reduction in accuracy relative to this configuration. Our results reveal that even a generous spacing of 4 cm with 10 tags on the string is sufficient to compute the unknown variables that fully-characterize each shape.

To have a more concrete understanding of what these errors mean, we visualize the results of one of the experiments: a concave shape with a 4cm inter-tag spacing, and tag position error of 1.6cm, shown in Fig 9b. We plot the 500 predictions of the different tags in different colors per tag with a transparency of 20%. The orange triangles are the ground truth positions of the fiducial markers. We first interpolate the fiducial markers' positions to infer the ground

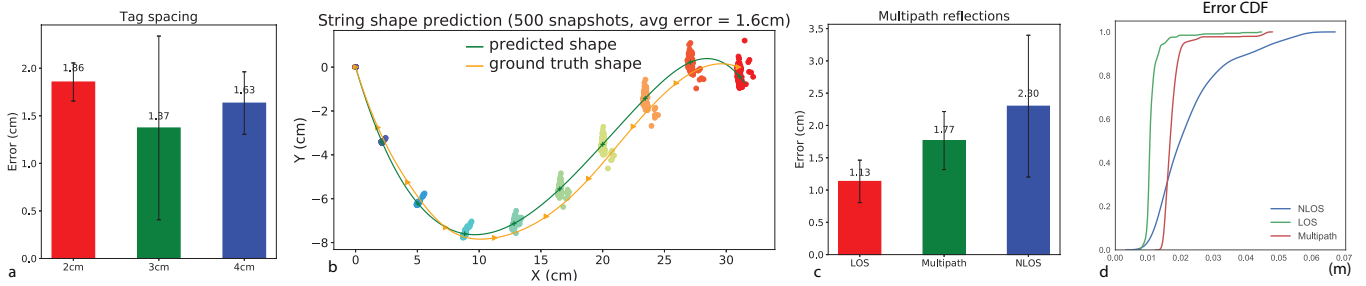Haojian Jin*, Jingxian Wang*, Zhijian Yang, Swarun Kumar, Jason Hong

Figure 9: Evaluation results: (a) The first graph shows the different errors in distance with 2 cm, 3 cm, 4cm tags spacing; (b) Predicted Shape; (c) Error in Distance under different wireless channel structure; (d) CDF of error in distance under LOS, NLOS, multipath.

truth shape (orange line). As we can see from Fig 9b, the shape prediction, with an average error at 1.6cm, is closely aligned with the ground truth shape, i.e., the predictions are largely close to the orange line. A random shape prediction can have a larger than 40 cm displacement error if we consider elasticity.

8.2 Signal Multipath

In the real world, we expect WiSh to disambiguate the multiple paths of the signals from the RFID tags to the reader as they reflect off walls, furniture, and even the user's own body. In this experiment, we evaluate the effect of signal multipath on WiSh.

Method: To evaluate the effect of signal multipath, we categorize the environments in which our experiment was conducted into three groups: direct line-of-sight (LOS, with minimal obstructions in the environment), multipath-rich settings (the presence of large metallic and other reflectors in the environment), non-line-of-sight (NLOS: RF signals traverse only through reflected paths to the tags). We only use the 1-D string prototype of RFID tags with a spacing of 3 cm for this experiment. For each multipath configuration, we test two classes of shapes (concave and wave) as described in §8.1.

Results: Figure 9c and 9d depict the error in tag position across the different radio environments. We observe a mean error of 1.13cm, 1.77cm and 2.30cm across the three classes of environments: line-of-sight, multipath, and non-line-of-sight, respectively. While the accuracy diminishes marginally in the absence of direct signal paths, WiSh remains largely robust to the multipath environments owing to the algorithms described in §5.2.

Partial Tag Observations: In the non-line-of-sight and multipath experiments, WiSh often cannot receive the responses from all RFID tags. As a result, WiSh will construct fewer equations than the line-of-sight experiments for the same number of unknown variables. Though WiSh can still reconstruct the surface shape from partial tag observations, it comes at the expense of accuracy.

8.3 Surface Materials

In this experiment, we evaluate the effect of fabric flexibility and test WiSh's performance under different types of stress in each instance: stretch and bend.

Method: We build four prototypes that accommodate stretch and bend using different types of fabric materials (Fig 10): latex rubber
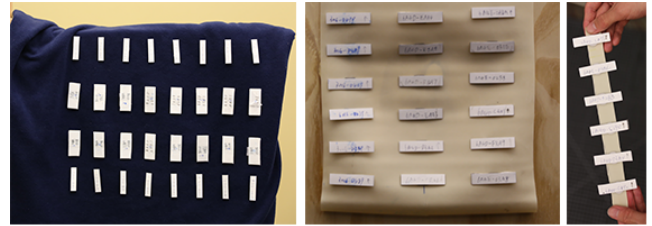

Figure 10: Surface material experiment apparatus: cotton surface, latex rubber surface, latex rubber string.
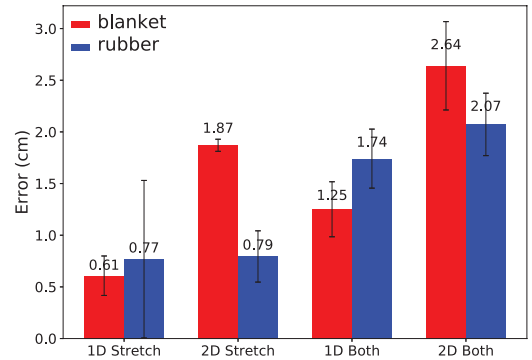

Figure 11: The mean tag position error across different materials and configurations

string (30cm), latex rubber surface (20cm × 20cm), cotton string (30cm), cotton surface (30cm × 40cm).

To evaluate stretch only, we hang the prototypes on a wood frame vertically and then hook different weights (0.5 kg and 1 kg) to the bottom of the prototype. Due to gravity, the strings/surfaces stretch differently. To test the stretch and bend at the same time, we stretch the prototypes slightly and place the prototypes on frames horizontally first and then attach weights on the surfaces or strings. We test convex, concave, wave shapes in each configuration. Unlike past experiments, the ground truth of shape deformation is captured by the fiducial tracking system in real-time to capture changes in shape over time.

Results: Figure 11 plots evaluation results for different types of materials. We observe an error between 0.5 cm-2.6 cm across different materials and different deformations, which indicates WiSh can work across various types of materials despite the presence
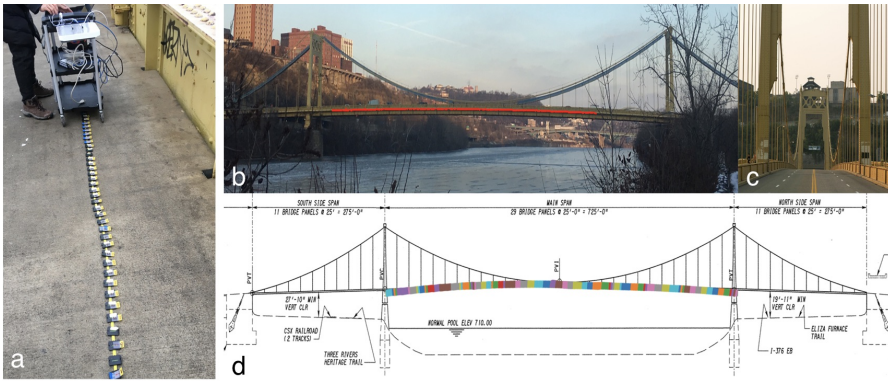
Figure 12: WiSh makes a 388-meter long bridge shape-aware. (a) We first build a measurement tape by sticking 50 RFID tags on a 5-meter string with an evenly 7cm tag spacing. A programmable iRobot drags the tape along the sidewalk of the main bridge span (b, c) Throughout the movement, WiSh continuously senses the tape curvature and stitches them together by intersecting the common areas. (d) The measurement is well aligned with the bridge schematic.
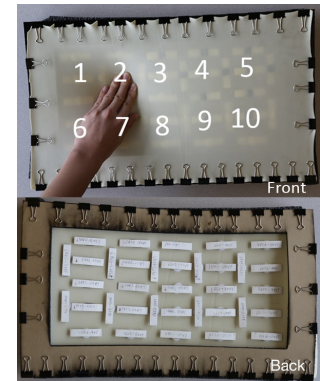

Figure 13: WiSh 10-key touchscreen prototype. We laser cut an acrylic board into a 40 cm x 20 cm frame, wrap the frame with a latex rubber surface and place 35 RFID tags on the back.

or absence of stretch. Among the different scenarios, the accuracy under both stretch and bend is poorer when compared to the accuracy under only stretch, primarily due to the more complex shapes that result. We also observe that WiSh requires more iterations to converge in its optimization algorithm to find the best solution in the "stretch and bend" scenario.

8.4   Aggregate Performance Under Stress

Finally, we present aggregate results from our measurements in the above experiments across various types of flexible surface materials (rubber, cotton, paper) across different environmental conditions (multipath rich, line-of-sight and non-line-of-sight).

Method: We measure system accuracy across over 20 experiments, each evaluating different types of shapes under: (1) Only stretch by attaching one weight at the extremity of the surface or string; (2) Both stretch and bending by attaching multiple weights to the surface and or string pulling along different directions.

Results: The below table lists the absolute mean errors in different configurations. In general, WiSh can sense the tag relative positions at a sub-centimeter accuracy and infer the fine-grained shape at 1 cm for a 0.4m string and 2 cm for a 0.3×0.4 m surface.

	Bend	Stretch	Both
String	13 mm	5.3 mm	17 mm
Surface	19 mm	8.7 mm	24 mm

9   APPLICATION SCENARIOS

This section describes results obtained from deploying WiSh for a variety of novel applications.

Shape-aware Bridges: Recent studies [17] have shown that one in 4 of US highway bridges - 60,000 of them - are either obsolete or in need of serious repair. However, routine visual inspections conducted by bridge engineers are costly and time-consuming [4, 14]. WiSh offers a potential solution for low-cost routine detection: sensing the fine-grained shape of a bridge by deploying RFID tags and mounting an RFID reader under an inspection vehicle.

Figure 14: Confusion Matrix of Touch Accuracy (%)

We run our experiment on a 388-meter long suspension bridge (Tenth Street Bridge [1]) in Downtown Pittsburgh (Fig. 12). To avoid potential license issue, we do not attach the RFID tags to the bridge directly. Instead, we build a measurement tape by sticking 50 RFID tags on a 5-meter string with an evenly 7cm tag spacing. We then use a programmable iRobot to drag the tape along the sidewalk of the main bridge span (220 m) at a constant speed.

During the process, WiSh continuously senses the tape curvature and re-associate shape predictions with bridge segments using the timestamps and movement speed. For each bridge segment, WiSh collects redundant shape measurements and averages them to remove the outliers and the influence of the ground (such as water ponds, potholes on the sidewalk). In the end, WiSh stitches the segments (visualized in different colors in Fig. 12d) by intersecting the common areas. Our measurements are well aligned with the officially reported bridge surveys.

3D Touch on Soft Surfaces: Figure 13 shows another example use case of WiSh: turning any soft object (e.g. toys, walls, etc.) into an interactive surface. By modeling the deformation of the shape, our system can infer the location and the pressure with which a user touches the surface. Our prototype implementation, shown in Fig. 13, divides the surface into ten touch areas and places 35 RFID tags on the back of the latex surface.

We perform four independent press actions at each key area (40 repetitions in total). Each press behavior lasts around 2 seconds, and WiSh collects at least ten snapshots for shape prediction. We use the shape deformation to infer the pressed key. The confusion matrix of touch point prediction accuracy (Fig. 14) shows that WiSh has a mean accuracy of 87%. The main errors occur because of ambiguity between neighboring touch areas. For example, touch area 1 is more likely to be confused with 2 and 6.

Spine Posture tracking: In this experiment, we consider a mobile user with a body-worn RFID reader and track RFID tags on the user's clothes. We deploy a linear tag array with 4cm of inter-tag spacing along the user's spine to measure posture. As before, we use the ARToolkit camera-based system as a baseline. Our results reveal a median error in the positions of the RFID tags of 17 mm. This demonstrates WiSh's high accuracy in the presence of body-worn tags and mobile readers.

Breath Sensing: Next, we repeat the above experiment with an additional one-dimensional RFID array along the user's chest. We ask the user to self-report breathing rate for 30 seconds, 12 times after exercises of different intensity. Our results find that WiSh can predict the user's breathing with a high accuracy of 95%.

Shape-aware Sofa/Chair/Carpet: We deploy our RFID tags on soft surfaces like chairs and carpet. Our experiments achieve a 92% accuracy in detecting the presence of person that is sitting or standing on the chair or carpet. This result shows a promising approach that can sense the presence of individuals by leveraging the extent of curvature of future carpets .

10 LIMITATIONS

While WiSh can infer a wide-variety of surface geometry, we highlight and discuss some important limitations:

Wrinkles: WiSh cannot obtain curvatures, such as wrinkles that are smaller than the dimensions of an RFID tag (3 cm). For instance, wrinkles that occur between two RFID tags may be virtually undetectable from the phases of the RFID tags alone.

Folds: WiSh cannot detect folds that cause some RFID tags to be placed upon others. This leads to near-field coupling between RFID tags that corrupts phase measurements on both tags, introducing large errors in our system.

Sensing and Computational Latency: Our WiSh prototype, running on a 2015 MacBook Pro, has an end-to-end refresh rate of around 2 Hz. This end-to-end refresh rate can be further decoupled into computation latency and raw signal reading latency. To reduce computation latency, we use a hybrid solution: we first find the initial shape using genetic algorithms ($\approx$ 5 seconds per search) and then search for the following shapes using a gradient descent approach ($\approx$ 0.3 second per search). The computing power of the RFID

reader determines the raw signal sampling rate. The Speedway reader (used in our evaluation) and ThingMagic6e (a commercial mobile reader) can process 3000/1000 readings per second, resulting in a refresh rate at 30/10 fps respectively for a 100-tag array.

Genetic algorithm: Our evaluation and recent Deep Genetic Learning research [45] show that the results of the genetic algorithm closely match that of a brute force search. False positives stem mainly from noise in the received signal. Adding more tags and Kalman filtering can reduce noise and the resulting false positives.

The tag density tradeoff: Increasing the number of RFID tags will improve the accuracy. However, doing so is limited by available space on fabric and tag's form factor. We do not study the specific relationship between model of tag, their density and the accuracy, since this relationship may not generalize across brands of tags [21].

11 DISCUSSION

Mobile Reader: In this paper, we envision a responsive environment using massively instrumented passive RFID tags, while the RFID reader would be mobile. These tags would be only activated if there is a nearby reader, e.g., a user, with a mobile reader in her pocket, interacts with a WiSh toy or steps on a WiSh carpet; a vehicle, with a reader installed, drives through a WiSh bridge.

This design may contradict the current RFID paradigm, where users carry RFID tags (e.g., RFID badges) and the always-on readers are stationary. Though our work is exploratory, we find this reversed architecture has several key advantages. First, mobile reader solutions can be more privacy-protective as users will have the control of RFID sensing [15]. Second, our proposed architecture is more cost-effective in settings such as smart homes, when the number of users is smaller than the number of objects need to be sensed.

Signal Collisions from Massive RFID tags: Signal collisions are a potential challenge if RFID tags are massively deployed in the environment. We currently use the default RFID protocol to resolve signal collisions. But the current RFID protocol is an overkill for WiSh since our retrieved tag IDs only need to be locally unique. Simplifying the RFID protocol and developing specialized backscatter tags will reduce collisions and increase the robustness significantly.

12 CONCLUSION

This paper presents WiSh, a system that enables RFID-based shape-aware smart surfaces. We present algorithms that track surface geometry from a compact single-antenna RFID reader that can be placed anywhere in the environment. Our system opens up a variety of applications: smart textiles that can report posture of the spine, interactive touch-sensitive toys and computer peripherals, and smart bridges that can detect their sag under stress. We present a prototype implementation and evaluation of WiSh on commodity Impinj RFID readers and tags, with our results showing promising accuracy in recovering the shape of a variety of surfaces in various multipath-rich settings.

REFERENCES

[1] 10th st (philip murray) bridge. http://historicbridges.org/bridges/browser/?bridgebrowser=pennsylvania/10th/. Accessed: 2018-04-25.

[2] Bézier curve - wikipedia. https://en.wikipedia.org/wiki/B%C3%A9zier_curve. (Accessed on 12/09/2017).

[3] Open source augmented reality sdk | artoolkit.org. https://www.artoolkit.org/. (Accessed on 12/07/2017).

[4] D. Agdas, J. A. Rice, J. R. Martinez, and I. R. Lasa. Comparison of visual inspection and structural-health monitoring as bridge condition assessment methods. *Journal of Performance of Constructed Facilities*, 30(3):04015049, 2015.

[5] A. Agrawal, G. J. Anderson, M. Shi, and R. Chierichetti. Tangible play surface using passive rfid sensor array. In *Extended Abstracts of the 2018 CHI Conference on Human Factors in Computing Systems*, CHI EA '18, pages D101:1–D101:4, New York, NY, USA, 2018. ACM.

[6] F. Ansari. *Sensing issues in civil structural health monitoring*. Springer, 2005.

[7] AtlasRFIDstore. Impinj rhcp far field rfid antenna (fcc/etsi). https://www.atlasrfidstore.com/impinj-rhcp-far-field-rfid-antenna-fcc-etsi/. (Accessed on 04/30/2018).

[8] L. Buechley. Sensormania - mediamatic. https://www.mediamatic.net/en/page/27491/sensormania, 2017. (Accessed on 11/29/2017).

[9] A. Dementyev, H.-L. C. Kao, and J. A. Paradiso. Sensortape: Modular and programmable 3d-aware dense sensor network on a tape. In *Proceedings of the 28th Annual ACM Symposium on User Interface Software & Technology*, pages 649–658. ACM, 2015.

[10] H. Ding, L. Shangguan, Z. Yang, J. Han, Z. Zhou, P. Yang, W. Xi, and J. Zhao. Femo: A platform for free-weight exercise monitoring with rfids. In *Proceedings of the 13th ACM Conference on Embedded Networked Sensor Systems*, pages 141–154. ACM, 2015.

[11] G. E. Farin. *Curves and surfaces for CAGD: a practical guide*. Morgan Kaufmann, 2002.

[12] S. Follmer, D. Leithinger, A. Olwal, N. Cheng, and H. Ishii. Jamming user interfaces: programmable particle stiffness and sensing for malleable and shape-changing devices. In *Proceedings of the 25th annual ACM symposium on User interface software and technology*, pages 519–528. ACM, 2012.

[13] N. S. Foundation. Futures of the scientific imagination | explore a safer, fashion-forward future. https://www.nsf.gov/news/special_reports/futures/. (Accessed on 11/29/2017).

[14] A. Gastineau, T. Johnson, and A. Schultz. Bridge health monitoring and inspections–a survey of methods. 2009.

[15] J. Hong. Toward a safe and secure internet of things - new america. https://www.newamerica.org/cybersecurity-initiative/policy-papers/toward-a-safe-and-secure-internet-of-things/, June, 2016. (Accessed on 05/03/2018).

[16] Y. Hou, Y. Wang, and Y. Zheng. Tagbreathe: Monitor breathing with commodity rfid systems. In *Distributed Computing Systems (ICDCS), 2017 IEEE 37th International Conference on*, pages 404–413. IEEE, 2017.

[17] C. Ingraham. Mapping america's most dangerous bridges - the washington post. https://www.washingtonpost.com/news/wonk/wp/2015/02/04/mapping-americas-most-dangerous-bridges/?utm_term=.d231413e97d3, 2015. (Accessed on 04/30/2018).

[18] R. Insider. Rfid readers for mobile phones from tsl. http://blog.atlasrfidstore.com/rfid-readers-mobile-phones-tsl, 2014.

[19] S. Izadi, D. Kim, O. Hilliges, D. Molyneaux, R. Newcombe, P. Kohli, J. Shotton, S. Hodges, D. Freeman, A. Davison, et al. Kinectfusion: real-time 3d reconstruction and interaction using a moving depth camera. In *Proceedings of the 24th annual ACM symposium on User interface software and technology*, pages 559–568. ACM, 2011.

[20] H. Jin, C. Xu, and K. Lyons. Corona: Positioning adjacent device with asymmetric bluetooth low energy rssi distributions. In *Proceedings of the 28th Annual ACM Symposium on User Interface Software & Technology*, UIST '15, pages 175–179, New York, NY, USA, 2015. ACM.

[21] H. Jin, Z. Yang, S. Kumar, and J. Hong. Towards wearable everyday body-frame tracking using passive rfids. *Proceedings of the ACM on Interactive, Mobile, Wearable and Ubiquitous Technologies*, 2017.

[22] T. Karrer, M. Wittenhagen, L. Lichtschlag, F. Heller, and J. Borchers. Pinstripe: eyes-free continuous input on interactive clothing. In *Proceedings of the SIGCHI Conference on Human Factors in Computing Systems*, pages 1313–1322. ACM, 2011.

[23] H. Li, E. Brockmeyer, E. J. Carter, J. Fromm, S. E. Hudson, S. N. Patel, and A. Sample. Paperid: A technique for drawing functional battery-free wireless interfaces on paper. In *Proceedings of the 2016 CHI Conference on Human Factors in Computing Systems*, CHI '16, pages 5885–5896, New York, NY, USA, 2016. ACM.

[24] H. Li, C. Ye, and A. P. Sample. Idsense: A human object interaction detection system based on passive uhf rfid. In *Proceedings of the 33rd Annual ACM Conference on Human Factors in Computing Systems*, pages 2555–2564. ACM, 2015.

[25] H. Li, P. Zhang, S. Al Moubayed, S. N. Patel, and A. P. Sample. Id-match: A hybrid computer vision and rfid system for recognizing individuals in groups. In

[26] H. Li, P. Zhang, S. Al Moubayed, S. N. Patel, and A. P. Sample. Id-match: A hybrid computer vision and rfid system for recognizing individuals in groups. In *Proceedings of the 2016 CHI Conference on Human Factors in Computing Systems*, pages 4933–4944. ACM, 2016.

[27] Y. Ma, N. Selby, and F. Adib. Minding the billions: Ultra-wideband localization for deployed rfid tags. In *ACM MobiCom*, 2017.

[28] P. Millot, L. Castanet, L. Casadebaig, N. Maaref, A. Gaugue, M. MÃŊnard, J. Khamlichi, G. Louis, N. Fortino, J. Y. Dauvignac, G. Clementi, M. Schortgen, L. Quellec, and V. Laroche. An uwb through-the-wall radar with 3d imaging, detection and tracking capabilities. In *2015 European Radar Conference (EuRAD)*, pages 237–240, Sept 2015.

[29] T. B. Moeslund and E. Granum. A survey of computer vision-based human motion capture. *Computer vision and image understanding*, 81(3):231–268, 2001.

[30] R. Nayak, A. Singh, R. Padhye, and L. Wang. Rfid in textile and clothing manufacturing: technology and challenges. *Fashion and Textiles*, 2(1):9, Jun 2015.

[31] G. Neumann, J. Garvin, J. B. Blair, Bufton, Jack, and B. Coyle. Lidar imaging of topography with millimeter ranging precision for proximity science and operations from rovers or spacecraft. 2017.

[32] H. N. Ng and R. L. Grimsdale. Computer graphics techniques for modeling cloth. *IEEE Computer Graphics and Applications*, 16(5):28–41, 1996.

[33] L. M. Ni, Y. Liu, Y. C. Lau, and A. P. Patil. Landmarc: indoor location sensing using active rfid. *Wireless networks*, 10(6):701–710, 2004.

[34] NPR. Time to overhaul america's aging bridges? https://www.npr.org/2012/08/31/160391678/time-to-overhaul-americas-aging-bridges, 2017. (Accessed on 04/24/2018).

[35] C. Occhiuzzi, S. Cippitelli, and G. Marrocco. Modeling, design and experimentation of wearable rfid sensor tag. *IEEE Transactions on Antennas and Propagation*, 58(8):2490–2498, 2010.

[36] P. Parzer, A. Sharma, A. Vogl, J. Steimle, A. Olwal, and M. Haller. Smartsleeve: Real-time monitoring of surface and deformation gestures on flexible, interactive textiles, using a hybrid gesture detection pipeline. In *Proceedings of the 30th Annual ACM Symposium on User Interface Software and Technology*, pages 565–577. ACM, 2017.

[37] N. Point. Optitrack. *Natural Point, Inc.,[Online]. Available: http://www. natural-point. com/optitrack/.[Accessed 22 2 2014]*, 2011.

[38] I. Poupyrev, N.-W. Gong, S. Fukuhara, M. E. Karagozler, C. Schwesig, and K. E. Robinson. Project jacquard: interactive digital textiles at scale. In *Proceedings of the 2016 CHI Conference on Human Factors in Computing Systems*, pages 4216–4227. ACM, 2016.

[39] S. Pradhan, E. Chai, K. Sundaresan, L. Qiu, M. A. Khojastepour, and S. Rangarajan. Rio: A pervasive rfid-based touch gesture interface. In *Proceedings of the 23rd Annual International Conference on Mobile Computing and Networking*, MobiCom '17, pages 261–274, New York, NY, USA, 2017. ACM.

[40] C. Rendl, D. Kim, S. Fanello, P. Parzer, C. Rhemann, J. Taylor, M. Zirkl, G. Scheipl, T. Rothländer, M. Haller, et al. Flexsense: a transparent self-sensing deformable surface. In *Proceedings of the 27th annual ACM symposium on User interface software and technology*, pages 129–138. ACM, 2014.

[41] S. Schneegass and A. Voit. Gesturesleeve: Using touch sensitive fabrics for gestural input on the forearm for controlling smartwatches. In *Proceedings of the 2016 ACM International Symposium on Wearable Computers*, pages 108–115. ACM, 2016.

[42] L. Shangguan, Z. Zhou, and K. Jamieson. Enabling gesture-based interactions with objects. In *Proceedings of the 15th Annual International Conference on Mobile Systems, Applications, and Services*, pages 239–251. ACM, 2017.

[43] M. Sherburn. *Geometric and mechanical modelling of textiles*. PhD thesis, University of Nottingham, 2007.

[44] T.-W. Shyr, J.-W. Shie, C.-H. Jiang, and J.-J. Li. A textile-based wearable sensing device designed for monitoring the flexion angle of elbow and knee movements. *Sensors*, 14(3):4050–4059, 2014.

[45] F. P. Such, V. Madhavan, E. Conti, J. Lehman, K. O. Stanley, and J. Clune. Deep neuroevolution: Genetic algorithms are a competitive alternative for training deep neural networks for reinforcement learning. *arXiv preprint arXiv:1712.06567*, 2017.

[46] D. Terzopoulos, J. Platt, A. Barr, and K. Fleischer. Elastically deformable models. In *ACM Siggraph Computer Graphics*, volume 21, pages 205–214. ACM, 1987.

[47] TexTrace. The textile rfid solution. http://www.textrace.com/en/index.php, 2017. (Accessed on 04/29/2018).

[48] M. Walter and A. Fournier. Approximate arc length parameterization. In *Proceedings of the 9th Brazilian symposium on computer graphics and image processing*, pages 143–150, 1996.

[49] H. Wang, J. Kearney, and K. Atkinson. Arc-length parameterized spline curves for real-time simulation. In *Proc. 5th International Conference on Curves and Surfaces*, pages 387–396, 2002.

[50] J. Wang, D. Vasisht, and D. Katabi. Rf-idraw: virtual touch screen in the air using rf signals. In *ACM SIGCOMM Computer Communication Review*, volume 44, pages

Haojian Jin*, Jingxian Wang*, Zhijian Yang, Swarun Kumar, Jason Hong

235–246. ACM, 2014.

[51] Y. Wang, C. C. Wang, and M. M. Yuen. Fast energy-based surface wrinkle modeling. *Computers & Graphics*, 30(1):111–125, 2006.

[52] T. Wei and X. Zhang. Gyro in the air: tracking 3d orientation of batteryless internet-of-things. In *Proceedings of the 22nd Annual International Conference on Mobile Computing and Networking*, pages 55–68. ACM, 2016.

[53] E. W. Weisstein. Rotation matrix. 2003.

[54] Wikipedia. Genetic algorithm. https://en.wikipedia.org/wiki/Genetic_algorithm, 2017. (Accessed on 12/07/2017).

[55] J. Xiong and K. Jamieson. Arraytrack: A fine-grained indoor location system. Usenix, 2013.

[56] L. Yang, Y. Chen, X.-Y. Li, C. Xiao, M. Li, and Y. Liu. Tagoram: Real-time tracking of mobile rfid tags to high precision using cots devices. In *Proceedings of the 20th annual international conference on Mobile computing and networking*, pages 237–248. ACM, 2014.

[57] L. Yao, R. Niiyama, J. Ou, S. Follmer, C. Della Silva, and H. Ishii. Pneui: Pneumatically actuated soft composite materials for shape changing interfaces. In *Proceedings of the 26th Annual ACM Symposium on User Interface Software and Technology*, UIST '13, pages 13–22, New York, NY, USA, 2013. ACM.

[58] L. Yao, J. Ou, C.-Y. Cheng, H. Steiner, W. Wang, G. Wang, and H. Ishii. Biologic: natto cells as nanoactuators for shape changing interfaces. In *Proceedings of the 33rd Annual ACM Conference on Human Factors in Computing Systems*, pages 1–10. ACM, 2015.

[59] W. Zhang, L. M. Sun, and S. W. Sun. Bridge-deflection estimation through inclinometer data considering structural damages. *Journal of Bridge Engineering*, 22(2):04016117, 2017.

[60] Y. Zhang, G. Laput, and C. Harrison. Electrick: Low-cost touch sensing using electric field tomography. In *Proceedings of the 2017 CHI Conference on Human Factors in Computing Systems*, CHI '17, pages 1–14, New York, NY, USA, 2017. ACM.

[61] Y. Zhu, Y. Yao, B. Y. Zhao, and H. Zheng. Object recognition and navigation using a single networking devic. 2017.